Neuron
Article

A Presynaptic ENaC Channel Drives Homeostatic Plasticity

Meg A. Younger,[1] Martin Müller,[1] Amy Tong,[1] Edward C. Pym,[1] and Graeme W. Davis[1,*]
[1]Department of Biochemistry and Biophysics, University of California, San Francisco, San Francisco, CA 94158-0822, USA
*Correspondence: graeme.davis@ucsf.edu
http://dx.doi.org/10.1016/j.neuron.2013.06.048

SUMMARY

An electrophysiology-based forward genetic screen has identified two genes, *pickpocket11* (*ppk11*) and *pickpocket16* (*ppk16*), as being necessary for the homeostatic modulation of presynaptic neurotransmitter release at the *Drosophila* neuromuscular junction (NMJ). Pickpocket genes encode Degenerin/Epithelial Sodium channel subunits (DEG/ENaC). We demonstrate that *ppk11* and *ppk16* are necessary in presynaptic motoneurons for both the acute induction and long-term maintenance of synaptic homeostasis. We show that *ppk11* and *ppk16* are co-transcribed as a single mRNA that is upregulated during homeostatic plasticity. Acute pharmacological inhibition of a PPK11- and PPK16-containing channel abolishes the expression of short- and long-term homeostatic plasticity without altering baseline presynaptic neurotransmitter release, indicating remarkable specificity for homeostatic plasticity rather than NMJ development. Finally, presynaptic calcium imaging experiments support a model in which a PPK11- and PPK16-containing DEG/ENaC channel modulates presynaptic membrane voltage and, thereby, controls calcium channel activity to homeostatically regulate neurotransmitter release.

INTRODUCTION

Homeostatic signaling systems are believed to interface with the mechanisms of learning-related plasticity to achieve stable, yet flexible, neural function and animal behavior. Experimental evidence from organisms as diverse as *Drosophila*, mouse, and humans demonstrates that homeostatic signaling systems stabilize neural function through the modulation of synaptic transmission, ion channel abundance, and neurotransmitter receptor trafficking (Petersen et al., 1997; Davis, 2006; Marder and Goaillard, 2006; Turrigiano, 2008; Thiagarajan et al., 2007; Kim and Ryan, 2010; Gonzalez-Islas et al., 2010). In each experiment, the cells respond to an experimental perturbation by modulating ion channel abundance or synaptic transmission to counteract the perturbation and re-establish baseline function. Altered homeostatic signaling is hypothesized to contribute to the cause or progression of neurological disease. For example, impaired or maladaptive homeostatic signaling may participate in the progression of autism-spectrum disorders (Ramocki and Zoghbi, 2008), Alzheimer's disease (Kamenetz et al., 2003), posttraumatic epilepsy (Davis and Bezprozvanny, 2001; Houweling et al., 2005), and epilepsy (Bernard et al., 2004; Jakubs et al., 2006).

The homeostatic modulation of presynaptic neurotransmitter release has been observed at mammalian central synapses (Piedras-Rentería et al., 2004; Kim and Ryan, 2010; Zhao et al., 2011) and at neuromuscular synapses in species ranging from *Drosophila* to mouse and human (Petersen et al., 1997; Frank et al., 2006; Davis, 2006; Plomp et al., 1992). The *Drosophila* neuromuscular junction (NMJ) is a prominent model system for the study of this form of homeostatic plasticity (Petersen et al., 1997; Davis and Goodman, 1998; Davis, 2006; Weyhersmüller et al., 2011). At the *Drosophila* NMJ, decreased postsynaptic neurotransmitter receptor sensitivity is precisely counteracted by a homeostatic potentiation of neurotransmitter release, thereby maintaining appropriate muscle excitation. The homeostatic enhancement of presynaptic release is due to increased vesicle release without a change in active zone number (Petersen et al., 1997; Frank et al., 2006; Müller et al., 2012). Throughout this manuscript, we refer to this process as "synaptic homeostasis," recognizing that it reflects a subset of homeostatic regulatory mechanisms that have been shown to stabilize neural function through modulation of ion channel gene expression and neurotransmitter receptor abundance (quantal scaling; Turrigiano, 2008; Marder and Goaillard, 2006).

We have pioneered an electrophysiology-based, forward genetic screen to identify the mechanisms of synaptic homeostasis (Dickman and Davis, 2009; Müller et al., 2011). To date, we have ascribed a role for several genes in the mechanism of synaptic homeostasis including the Eph receptor (Frank et al., 2006), the schizophrenia-associated gene *dysbindin* (Dickman and Davis, 2009), the presynaptic CaV2.1 calcium channel (Frank et al., 2006, 2009), presynaptic Rab3 GTPase-activating protein (Rab3-GAP; Müller et al., 2011), and Rab3-interacting molecule (RIM; Müller et al., 2012). An emerging model suggests that, in response to inhibition of postsynaptic glutamate receptor function, a retrograde signal acts upon the presynaptic nerve terminal to enhance the number of synaptic vesicles released per action potential to precisely offset the severity of glutamate receptor inhibition. Two components of the presynaptic release mechanism are necessary for the execution of synaptic homeostasis, increased calcium influx through presynaptic CaV2.1 calcium channels (Müller and Davis, 2012) and a RIM-dependent increase in the readily releasable pool of synaptic vesicles

(Müller et al., 2012). Many questions remain unanswered. In particular, how is a change in presynaptic calcium influx induced and sustained during synaptic homeostasis?

Here, we report the identification of two genes, *pickpocket16* (*ppk16*) and *pickpocket11* (*ppk11*), that, when mutated, block homeostatic plasticity. *Drosophila* pickpocket genes encode Degenerin/Epithelial Sodium channel (DEG/ENaC) subunits (Adams et al., 1998; Liu et al., 2003a; Bianchi and Driscoll, 2002). Channels in this superfamily are voltage insensitive and are assembled as either homomeric or heteromeric trimers (Bianchi and Driscoll, 2002; Benson et al., 2002; Jasti et al., 2007). Each channel subunit has two transmembrane domains with short cytoplasmic N and C termini and a large extracellular loop implicated in responding to diverse extracellular stimuli.

Little is known regarding the function of pH-insensitive DEG/ENaC channels in the nervous system. DEG/ENaC channels have been implicated as part of the mechanotransduction machinery (Chalfie, 2009) and in taste perception in both invertebrate and vertebrate systems (Liu et al., 2003b; Chandrashekar et al., 2010). In *Drosophila*, PPK11 has been shown to function as an ENaC channel subunit that is required for the perception of salt taste (Liu et al., 2003b) and fluid clearance in the tracheal system, a function that may be considered analogous to ENaC channel activity in the mammalian lung (Liu et al., 2003a).

We demonstrate that *ppk11* and *ppk16* are coregulated during homeostatic synaptic plasticity and that homeostatic plasticity is blocked when gene is genetically deleted, when gene expression is disrupted in motoneurons, or when pickpocket channel function is pharmacologically inhibited. We then take advantage of the fact that presynaptic homeostasis can be blocked pharmacologically to demonstrate that the persistent induction of homeostatic plasticity does not interfere with synapse growth and development. We show that homeostatic plasticity can be acutely and rapidly erased, leaving behind otherwise normal synaptic transmission. Finally, we demonstrate that pharmacological inhibition of this pickpocket channel abolishes the homeostatic modulation of presynaptic calcium influx that was previously shown to be necessary for the homeostatic increase in neurotransmitter release (Müller and Davis, 2012).

A model for DEG/ENaC channel function can be based on the well-established regulation of ENaC channel trafficking in the kidney during the homeostatic control of salt balance. Enhanced sodium reabsorption in the principle cells of the cortical collecting duct of the kidney is achieved by increased ENaC channel transcription and trafficking to the apical cell surface, which enhances sodium influx. Sodium is then pumped out of the basolateral side of the cell, accomplishing sodium reabsorption (Schild, 2010). By analogy, we propose a model for synaptic homeostasis in which the trafficking of DEG/ENaC channels to the neuronal membrane, at or near the NMJ, modulates presynaptic membrane potential to potentiate presynaptic calcium channel activity and thereby achieve precise homeostatic modulation of neurotransmitter release.

RESULTS

We are pursuing an ongoing electrophysiology-based forward genetic screen for mutations that block the rapid induction of synaptic homeostasis. In brief, we record from the NMJ of annotated transposon-insertion mutations in the presence of the glutamate receptor antagonist philanthotoxin-433 (PhTx; 10 μM) according to published methods (Dickman and Davis, 2009; Müller et al., 2011). For each NMJ, we quantify miniature excitatory postsynaptic potential (mEPSP) amplitude, EPSP amplitude, quantal content (calculated by dividing the EPSP amplitude/mEPSP amplitude), mEPSP frequency, muscle input resistance, and muscle resting membrane potential. In wild-type (WT), the application of PhTx induces a homeostatic increase in presynaptic release that restores EPSP amplitudes to wild-type levels (0.5 mM Ca^{2+}). We are then able to identify mutations that have a reduced EPSP amplitude in the presence of PhTx and therefore appear to disrupt homeostatic plasticity. To further validate our screen, we analyzed a subset of mutations in the presence and absence of PhTx, regardless of whether or not they appeared to block synaptic homeostasis. In Figure 1A, we present data for a sample of 22 transposon insertion lines in which synaptic transmission was assayed both in the absence and in the presence of PhTx (mutation annotations are listed in Table S1 available online; sample sizes are 3–14 muscles for each genotype in each condition). For each genotype, we present the percent change in mEPSP amplitude as an indication of the severity of glutamate receptor inhibition (black bars), as well as the percent change in quantal content (gray bars), which indicates the magnitude of the homeostatic increase in presynaptic release. In all cases, mEPSP amplitude is reduced and most mutants are capable of robust homeostatic plasticity (Dickman and Davis, 2009; Müller et al., 2011). Notably, the transposon insertion lines that we screened showed a wide range of baseline-evoked responses in the absence of PhTx (Figure 1B), with EPSP amplitudes ranging between 18.0 ± 2.5 mV (*CcapR*, n = 6) and 43.0 ± 2.3 mV (nAChRα-18C, n = 4). Despite the considerable span in baseline release, most transposon insertion lines were capable of synaptic homeostasis, as indicated by a PhTx-dependent increase in quantal content (Figure 1A). However, a few lines showed virtually no PhTx-dependent change in quantal content, indicating impaired homeostatic compensation. The mutation in *rab3-GAP* has been previously published and is a confirmed homeostatic plasticity gene (Figure 1A, green bars; Müller et al., 2011). Another line that showed a decrease in mEPSP amplitude, but no increase in presynaptic release, resides within the *ppk11* gene locus (Figure 1A, blue bars). *ppk11* was, therefore, selected as a candidate homeostatic plasticity gene.

In order to pursue a formal genetic analysis of *ppk11*, we acquired additional genetic and transgenic reagents (Figure 1C). These reagents include: (1) an independently derived Minos transposable element insertion ($ppk11^{Mi}$) that resides within a coding exon of the *ppk11* gene and is predicted to be a strong loss-of-function or null mutation, (2) a previously published *UAS-ppk11-RNAi* transgenic line (Liu et al., 2003b), (3) a previously published dominant-negative transgene (*UAS-dnPPK11*; Liu et al., 2003b) targeting the PPK11 trimerization domain that disrupts channel assembly, and (4) a deficiency chromosome (Df) that uncovers the entire *ppk11* gene locus.

The *ppk11* gene terminates in close proximity (63 bp upstream) to the predicted start of another member of the

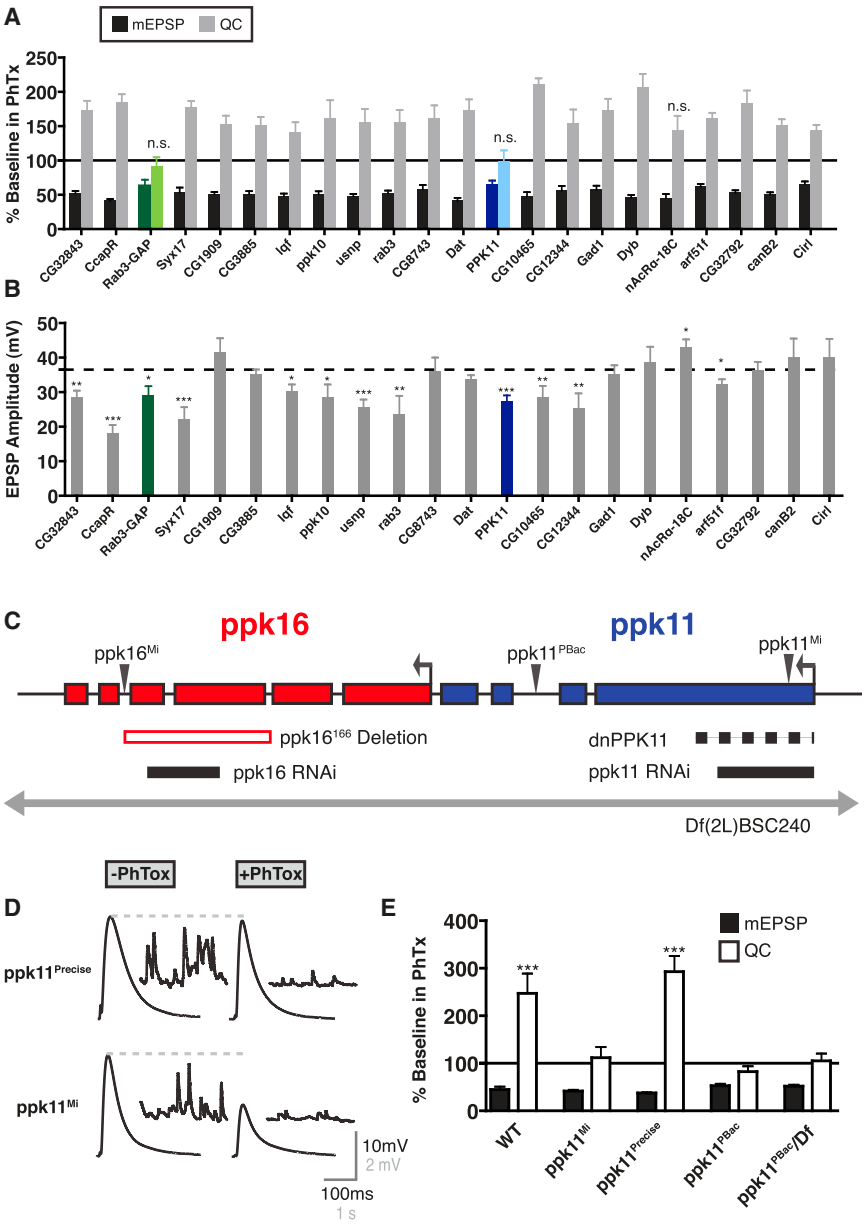

Figure 1. *ppk11* Is Necessary for the Homeostatic Modulation of Presynaptic Neurotransmitter Release

(A) The percent change in mEPSP amplitude (black bars) and quantal content (QC; gray bars) in the presence of PhTx relative to baseline for each genotype in the absence of PhTx. The $ppk11^{PBac}$ mutation is shown in blue and the *rab3-GAP* mutation is shown in green. All changes in mEPSP are significant ($p < 0.01$) as are changes in EPSP amplitude ($p \leq 0.05$) unless indicated otherwise.

(B) Average EPSP amplitude is plotted for each genotype shown in (A) in the absence of PhTx.

(C) Schematic showing the genetic locus that includes *ppk11* (blue) and *ppk16* (red). Transposon insertion sites are indicated by black arrowheads, regions targeted by RNAi are indicated by black lines, the *dnPPK11* construct is indicated by a dotted line, the $ppk16^{166}$ deletion is indicated by an open red bar, and a deficiency spanning the locus is shown as a gray arrow.

(D) Representative traces showing EPSPs and mEPSPs from $ppk11^{Precise}$ (top) and $ppk11^{Mi}$ (bottom). All genotypes are shown without and with PhTx (left and right, respectively).

(E) The percent change in mEPSP (solid bars) and quantal content (QC; open bars) in the presence of PhTx relative to baseline for each genotype recorded in the absence of PhTx. All conditions show a significant decrease in mEPSP amplitude ($p < 0.001$). Only wild-type (WT) and the precise excision ($ppk11^{Precise}$) show an increase in quantal content ($p < 0.001$). All data are recorded in 0.3–0.35 mM extracellular calcium (see Table S1). Data are presented as average ± SEM. Comparisons are made according to a Student's t test.

DEG/ENaC channel family, *pickpocket16* (*ppk16*) (Figure 1C, red). The close proximity of these two genes suggested that they might both contribute to the same DEG/ENaC channel. Therefore, we assembled genetic reagents to test the hypothesis that PPK16 might function with PPK11 during synaptic homeostasis. These reagents include: (1) a Minos transposon insertion that resides within the *ppk16* gene ($ppk16^{Mi}$), (2) a newly generated small deficiency ($ppk16^{166}$) that removes two coding exons of the *ppk16* gene and is predicted to be a strong loss-of-function or null mutation, and (3) a *UAS-ppk16-RNAi* transgenic line. Together, these reagents allow us to test the involvement of both *ppk11* and *ppk16* during synaptic homeostasis.

Loss of *ppk11* Blocks the Rapid Induction of Synaptic Homeostasis

To examine the rapid induction of synaptic homeostasis, we applied PhTx (10–20 μM) to the dissected NMJ for 10 min (see Experimental Procedures) and made recordings from muscle 6 in abdominal segments A2 and A3. For purposes of display, data for a given mutant background are presented as normalized to the same genotype recorded in the absence of PhTx, as done previously (Frank et al., 2006, 2009; Bergquist et al., 2010). All of our data are also presented as non-normalized values (Table S2). In wild-type, application of PhTx causes a significant decrease in mEPSP amplitude compared to baseline and we observe a homeostatic increase in presynaptic neurotransmitter release (Figure 1E). However, in mutations that disrupt the *ppk11* gene, we find that synaptic homeostasis is completely and consistently blocked. Specifically, in every mutation that we have analyzed, including the homozygous $ppk11^{Mi}$ mutation, the homozygous $ppk11^{PBac}$ mutation, and $ppk11^{PBac}/Df$, there is no statistically significant increase in presynaptic neurotransmitter release after PhTx-dependent inhibition of mEPSP amplitudes. We also generated a precise excision

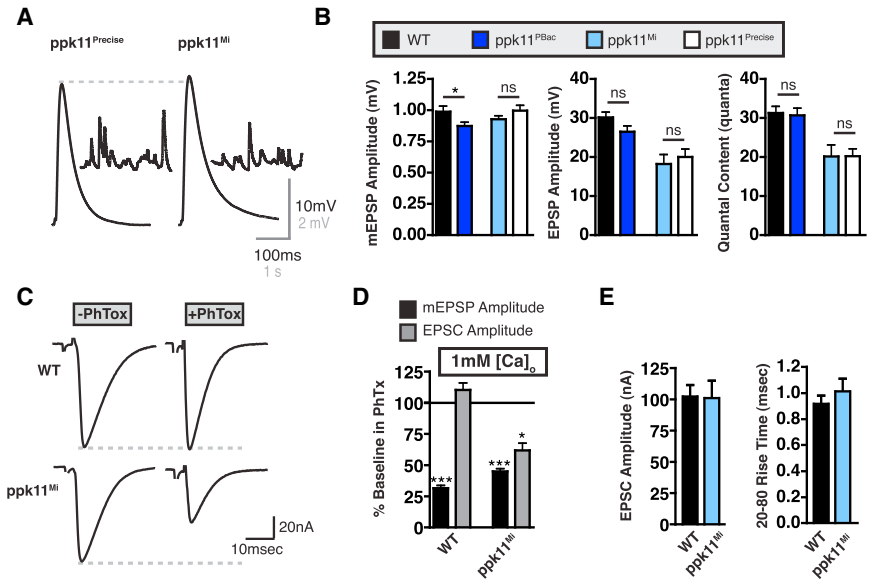

Figure 2. Analysis of Baseline Neurotransmission in *ppk11* Mutants

(A) Sample traces for the indicated genotypes.

(B) mEPSP amplitude, EPSP amplitude, and quantal content for wild-type (WT), *ppk11*^{PBac}, *ppk11*^{Mi}, and *ppk11*^{Precise} at 0.35 mM extracellular calcium.

(C) Representative examples of EPSCs from wild-type (WT; top) and *ppk11*^{Mi} (bottom) in the absence of PhTx (left) and presence of PhTx (right) at 1 mM extracellular calcium.

(D) Percent change in mEPSP amplitude and EPSC amplitude in the presence of PhTx compared to baseline in the absence of PhTx for each genotype. EPSC amplitude is not altered in WT after the addition of PhTx ($p = 0.39$), demonstrating homeostatic compensation (102.3 ± 9.2 nA, n = 5 without PhTx and 112.8 ± 5.8 nA, n = 4 with PhTx). EPSC amplitude is significantly reduced in *ppk11*^{Mi} after the addition of PhTx ($p < 0.05$), demonstrating impaired homeostatic compensation (101.0 ± 13.9 nA, n = 8 without PhTx and 62.4 ± 5.9 nA, n = 9 with PhTx).

(E) In the absence of PhTx, neither EPSC amplitude nor EPSC 20%–80% rise time is different compared to WT ($p = 0.95$ and $p = 0.48$, respectively). Data are presented as average ± SEM. Comparisons are made according to a Student's t test.

of the *ppk11*^{Mi} transposon that restores the *ppk11* gene locus, assessed by sequence analysis. After the addition of PhTx to the precise excision background (*ppk11*^{Precise}), the EPSP amplitude is returned to the size it was in the absence of PhTx (*ppk11*^{Precise}; Figure 1D), and the homeostatic enhancement of presynaptic neurotransmitter release is restored to wild-type levels (Figure 1E). Taken together, these data support the conclusion that disruption of the *ppk11* gene blocks the rapid induction of synaptic homeostasis.

Despite observing a complete block of synaptic homeostasis, there is no consistent alteration in baseline synaptic transmission caused by the loss of *ppk11*. First, we compare wild-type (Figure 2B, black bars) with the *ppk11*^{PBac} mutation (Figure 2B, dark blue bars) and find no significant change in presynaptic release and only a minor change in mEPSP amplitude. Second, we compare the *ppk11*^{Mi} mutation (Figure 2B, light blue bars) with its appropriate genetic control, the precise excision of the *ppk11*^{Mi} transposon (*ppk11*^{Precise}; Figure 2B, open bars). There is no change in baseline release when this comparison is made. We note that there is a significant ($p < 0.01$) difference in baseline release when we compare wild-type with either *ppk11*^{Mi} or the *ppk11*^{Precise} control line, and we attribute this to differences in genetic background. Third, we analyzed a *trans*-heterozygous combination of independently derived *ppk11* mutations (*ppk11*^{Mi}/ *ppk11*^{PBac}) and find no change in quantal content compared to wild-type (Figure S1). In this *trans*-heterozygous combination, there is a decrease in mEPSP amplitude that correlates with a decrease in postsynaptic muscle input resistance (WT = 8.1 MΩ compared to *ppk11*^{Mi}/ *ppk11*^{PBac} = 3.9 MΩ; $p < 0.01$). From these data, we conclude that disruption of *ppk11* blocks synaptic homeostasis without altering baseline release, specifically when mutations are compared to their appropriate genetic control. This conclusion is supported by several additional experiments, presented below.

We next examined synaptic homeostasis and baseline transmission at elevated external calcium (1 mM) that is within the range of what is thought to be physiological calcium (Figures 2C–2E). We first quantified mEPSP amplitudes in current-clamp mode, in which the signal-to-noise ratio is excellent, and then switched to two-electrode voltage-clamp mode to measure evoked synaptic currents. We observe a decrease in mEPSP amplitude when PhTx is applied to the wild-type NMJ at 1 mM calcium and we find that EPSC amplitudes are unchanged in the presence of PhTx, as expected for precise homeostatic compensation. However, in the *ppk11*^{Mi} mutant, a similar decrease in mEPSP amplitude is achieved after PhTx application, but the average EPSC amplitude remains significantly smaller than the average baseline EPSC recorded in the absence of PhTx. Thus, homeostatic compensation is disrupted in the *ppk11*^{Mi} mutant at physiological calcium without a parallel deficit in baseline transmission. Taken together with our results from Figure 1, these data show that synaptic homeostasis is blocked at two different extracellular calcium concentrations (0.3 mM and 1 mM). Finally, it is also worth noting that we observed a significant decrease in muscle input resistance in the *ppk11*^{PBac}, the *ppk11*^{Mi} mutant, and the *ppk11*^{Precise} control compared to wild-type, indicating an effect in the muscle cell, although the persistence of this effect in the *ppk11*^{Precise} control suggests that it is also not linked to this genetic locus and cannot account for a change in homeostatic plasticity (Table S2).

ppk11 Is Necessary in Motoneurons for the Rapid Induction of Synaptic Homeostasis

To confirm that *ppk11* is necessary for the rapid induction of synaptic homeostasis, and to determine whether PPK11 functions in motoneurons or muscle (or both), we took advantage of both a previously published *UAS-ppk11-RNAi* line and a previously published dominant-negative transgene that targets PPK11

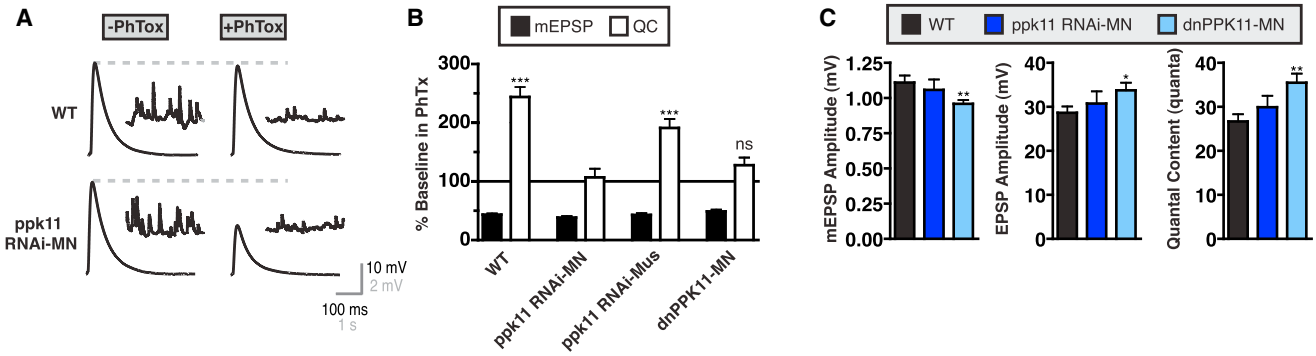

Figure 3. *ppk11* Is Required in Motoneurons for Synaptic Homeostasis

(A) Sample traces for the indicated genotypes.

(B) Percent change in mEPSP (filled bars) and QC (open bars) as in Figure 1E. mEPSP amplitude is decreased after the addition of PhTx in all conditions ($p < 0.001$). WT and *UAS-ppk11-RNAi* driven in muscle (*MHC-GAL4*) show a significant increase in quantal content (QC; $p < 0.001$). *UAS-ppk11-RNAi* and *UAS-dnPPK11* driven in motoneurons (*OK371-GAL4*) show no significant increase in QC after PhTx treatment ($p = 0.69$ and $p = 0.09$, respectively), demonstrating impaired synaptic homeostasis.

(C) mEPSP amplitude, EPSP amplitude, and quantal content are shown. mEPSP amplitude is unchanged in the *UAS-ppk11-RNAi* driven in motoneurons and reduced in the *UAS-dnPPK11* driven in motoneurons ($p < 0.01$). There is no decrease in EPSP amplitude or quantal content when either transgenic condition is compared to wild-type. There is a small but significant increase in EPSP amplitude ($p < 0.05$) and quantal content ($p < 0.01$) when *UAS-dnPPK11* is driven in motoneurons. Data are presented as average ± SEM. Comparisons are made according to a Student's t test.

(Liu et al., 2003b). First, we demonstrate that expression of *UAS-ppk11-RNAi* selectively in motoneurons (*OK371-GAL4*) completely blocks the homeostatic increase in presynaptic release after PhTx-dependent inhibition of postsynaptic glutamate receptors (Figures 3A and 3B). By contrast, expression of *UAS-ppk11-RNAi* in muscle (*MHC-GAL4*) does not (Figure 3B). These data indicate that *ppk11* is required in motoneurons for synaptic homeostasis. Because *ppk11* is expressed in *Drosophila* trachea, where it has been implicated in fluid clearance, we visually confirmed that *OK371-GAL4* does not express in trachea by driving *UAS-CD8-GFP* (data not shown). Next, we attained independent confirmation that PPK11 functions in motoneurons during homeostatic plasticity by expressing the *UAS-dnPPK11* transgene in motoneurons with *OK37-GAL4*. Again, we observe a complete block of homeostatic compensation (Figure 3B). Notably, the motoneuron-specific expression of *UAS-ppk11-RNAi* blocks synaptic homeostasis without altering any aspect of synaptic transmission in the absence of PhTx (Figure 3C). When the *UAS-dnPPK11* transgene is expressed in motoneurons, there is a small decrease in mEPSP amplitude and a small increase in quantal content, neither of which is of a magnitude that is expected to interfere with homeostatic plasticity. Based on these data, we conclude that *ppk11* is necessary in motoneurons for synaptic homeostasis and that the blockade of synaptic homeostasis is independent of any effect of PPK11 on baseline synaptic transmission.

ppk16 Is Necessary for the Rapid Induction of Synaptic Homeostasis

To determine whether *ppk16* is required for synaptic homeostasis, we examined a Minos transposon insertion that resides within an intron of the *ppk16* gene ($ppk16^{Mi}$; Figure 1C). After the addition of PhTx, we observed a complete block in synaptic homeostasis (Figures 4A and 4B). To confirm this finding, we utilized imprecise excision of the $ppk16^{Mi}$ element to generate a deletion mutation that removes 767 base pairs of the *ppk16* gene, encompassing a large portion of the predicted extracellular domain (Figure 1C). This deletion mutation, termed $ppk16^{166}$, is expected to be a strong loss-of-function or null allele. We find that the $ppk16^{166}$ mutation also blocks synaptic homeostasis (Figure 4B). Finally, significant synaptic homeostasis is restored in animals with a precise excision of the $ppk16^{Mi}$ transposon (158% increase in release; $p < 0.05$ compared to the same genotype in the absence of PhTx), indicating that the block in synaptic homeostasis is derived from this genetic locus.

To confirm that *ppk16* is necessary for synaptic homeostasis, and to determine whether it is required in motoneurons along with *ppk11*, we expressed *UAS-ppk16-RNAi* in either motoneurons or muscle. When expressed in motoneurons, *UAS-ppk16-RNAi* completely blocks synaptic homeostasis (Figures 4D and 4E). However, muscle-specific expression does not (Figure 4E). Furthermore, expression of *UAS-ppk16-RNAi* blocks synaptic homeostasis without altering baseline EPSP amplitude or presynaptic vesicle release (quantal content; Figure 4F). Although there is a small but statistically significant change in mEPSP amplitude, this minor deficit is unlikely to account for the complete block of the homeostatic modulation of quantal content. Taken together, these data support the conclusion that *ppk16* is necessary in motoneurons for homeostatic plasticity and could function with PPK11 in a novel DEG/ENaC channel that is required for synaptic homeostasis.

We performed an additional experiment to explore the potential subunit composition of the putative motoneuron DEG/ENaC channel. Pickpocket19 (PPK19) has been previously implicated in acting with PPK11 in the taste cells of the terminal organ (Liu et al., 2003b). A *UAS-ppk19-RNAi* was previously shown to inhibit sodium preference when expressed in sensory neurons (Liu et al., 2003b). However, when this RNAi is expressed in motoneurons, homeostasis remains normal (Figure 4E). These data suggest that PPK19 is unlikely to be a third subunit of

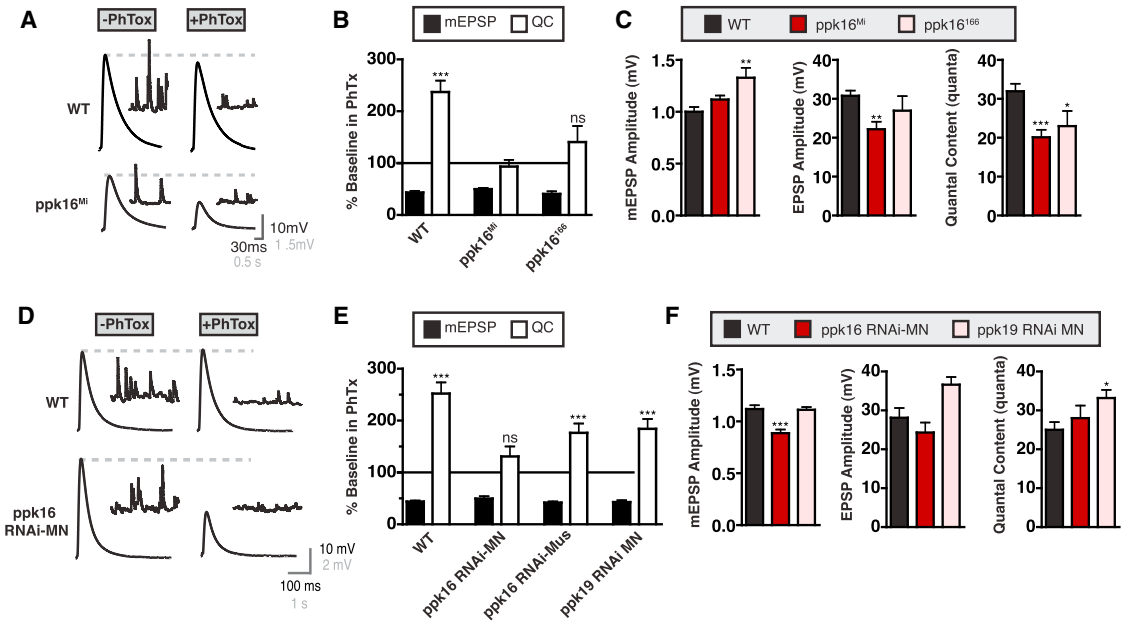

Figure 4. *ppk16* Is Necessary in Motoneurons for the Homeostatic Modulation of Presynaptic Release

(A) Sample traces for the indicated genotypes.

(B) Percent change in mEPSP (filled bars) and quantal content (QC; open bars) as in Figure 1D. mEPSP amplitude is decreased after the addition of PhTx in all conditions ($p < 0.001$). WT shows an increase in QC ($p < 0.001$), while $ppk16^{Mi}$ and $ppk16^{166}$ do not ($p = 0.68$ and $p = 0.24$, respectively).

(C) mEPSP amplitude, EPSP amplitude, and QC are shown. $ppk16^{166}$ has an increased mEPSP amplitude ($p < 0.01$) compared to WT. $ppk16^{Mi}$ and has decreased EPSP amplitude compared to WT ($p < 0.001$). $ppk16^{Mi}$ and $ppk16^{166}$ show reduced QC ($p < 0.001$ and $p < 0.05$, respectively) compared to WT.

(D) Sample traces for the indicated genotypes.

(E) Data are as in (B). mEPSP amplitude is decreased after the addition of PhTx in all conditions ($p < 0.001$). WT, *UAS-ppk16-RNAi* driven in the muscle (*MHC-GAL4*), and *UAS-ppk19-RNAi* driven in motoneurons (*OK371-GAL4*) show an increase in QC ($p < 0.001$), demonstrating normal synaptic homeostasis. *UAS-ppk16-RNAi* driven in motoneurons (*OK371-GAL4*) does not show an increase in QC, demonstrating a block of synaptic homeostasis ($p = 0.19$).

(F) Data are as in (C). mEPSP amplitude is decreased when the *UAS-ppk16-RNAi* is expressed in motoneurons ($p < 0.001$), while EPSP amplitude and quantal content remain unchanged ($p = 0.30$ and $p = 0.44$, respectively). There is an increase in EPSP amplitude and quantal content ($p < 0.05$) when *UAS-PPK19-RNAi* is expressed in motoneurons. Data are presented as average ± SEM. Comparisons are made according to a Student's t test.

the putative DEG/ENaC channel required for synaptic homeostasis.

As observed in *ppk11* mutants, loss of *ppk16* has a relatively minor effect on baseline synaptic transmission. Although we observe a significant decrease in EPSP amplitude and quantal content in the homozygous $ppk16^{Mi}$ transposon mutant, we find that baseline transmission is unaltered when compared to the *ppk16* precise excision mutant, which is the appropriate genetic control (20.1 ± 1.9 and 26.2 ± 3.3 quanta, respectively, $p = 0.11$). Consistent with this conclusion, the deletion mutation ($ppk16^{166}$) shows a wild-type EPSP amplitude, composed of a mEPSP that is slightly larger than wild-type and a quantal content that is slightly smaller than wild-type (Figure 4C). Finally, motoneuron-specific expression of *UAS-ppk16-RNAi* does not alter quantal content but blocks homeostatic plasticity (Figure 4F). The emerging picture is that loss of *ppk16* does not cause a consistent or dramatic defect in presynaptic release, but synaptic homeostasis is severely perturbed.

ppk11 and *ppk16* Mutations Do Not Alter NMJ Growth or Morphology

To determine whether either *ppk11* or *ppk16* participate in anatomical NMJ development, we quantified the number of synaptic boutons at muscle 6/7, the NMJ at which all of our electrophysiological recordings were performed. In abdominal segment 2, no changes were observed in $ppk11^{PBac}$ and a small increase was observed in $ppk16^{Mi}$ compared to wild-type (120.3% ± 9.9% of wild-type, $p < 0.05$; Figure 5B). We also quantified morphology at abdominal segment 3 and found no significant differences in either *ppk11* or *ppk16* mutants (data not shown). Next, we examined the NMJ of muscle 4, which is situated in the middle of the muscle, making it ideal for visualizing all active zones within each NMJ by staining for the presynaptic active-zone-associated protein Bruchpilot (Brp; Davis et al., 1997; Wagh et al., 2006). Mutations in *ppk11* or *ppk16* had no significant effect on NMJ area, determined by staining for the PSD-95 homolog Discs Large (DLG), and no significant change in the number of active zones per NMJ (Figures 5C and 5D). When we calculated active zone density by dividing active zone number by NMJ area, we find no change in $ppk11^{PBac}$ and a small (8.4% ± 2.4%, $p < 0.05$ compared to wild-type) decrease in $ppk16^{Mi}$ (Figure 5E). Since there were no major changes in NMJ appearance, size, or organization, we conclude that neither *ppk11* nor *ppk16* plays a prominent role in NMJ growth.

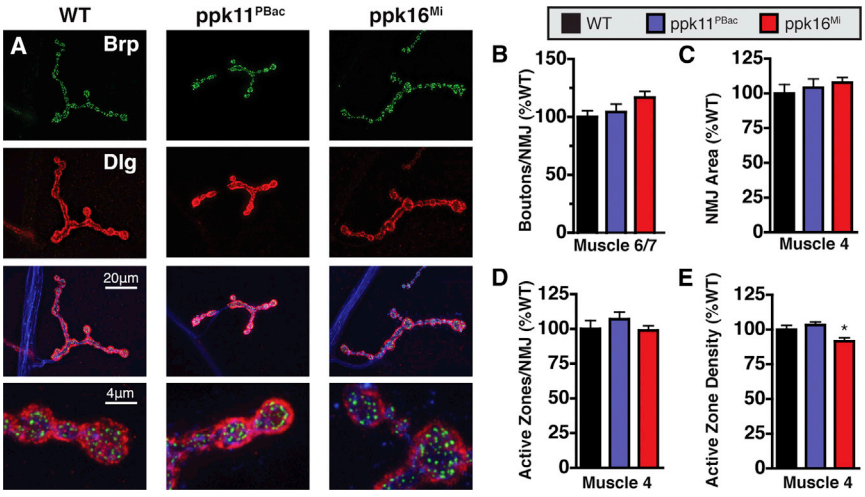

Figure 5. Normal NMJ Morphology in *ppk11* and *ppk16* Mutants

(A) Representative images of from muscle 4 of wild-type (WT), *ppk11*^{PBac}, and *ppk16*^{Mi} mutant animals stained for BRP (green), DLG (red), and HRP (blue). The bottom panel shows boutons enlarged 5×.

(B) The number of boutons per NMJ at muscles 6/7 in segment 2 is expressed as percent wild-type (% WT) bouton number. No significant changes were observed.

(C) The area of the NMJ at muscle 4 is shown as percent WT area, as measured by DLG staining. It is not significantly different from wild-type in either genotype.

(D) The number of active zones per NMJ at muscle 4 is shown as the percent WT active zones (measured as individual Brp puncta). Active zone number is not different from WT in either genotype.

(E) The active zone density at muscle 4 is shown as percent WT active zone density. There is no significant difference in *ppk11*^{PBac}, and a small decrease is observed in *ppk16*^{Mi} ($p < 0.05$). Data are presented as average ± SEM. Comparisons are made according to a Student's t test.

ppk11 Is Required for the Sustained Expression of Synaptic Homeostasis

Genetic deletion of the muscle-specific glutamate receptor subunit GluRIIA (*GluRIIA*^{SP16}) has been shown to decrease mEPSP amplitudes by ~50% and induce a homeostatic increase in presynaptic release that restores EPSP amplitudes to wild-type levels (Petersen et al., 1997; DiAntonio et al., 1999; Frank et al., 2006; Figures 6A and 6B). Since the *GluRIIA* mutation is present throughout larval development, this experiment reflects the sustained expression of synaptic homeostasis for several days. To test whether *ppk11* is necessary for the sustained expression of synaptic homeostasis, we generated a *GluRIIA*^{SP16}, *ppk11*^{PBac} double mutant. The double mutant shows a decrease in mEPSP amplitude without a homeostatic increase in presynaptic release (Figures 6A and 6B), demonstrating that *ppk11* is necessary for both the rapid induction and the sustained expression of synaptic homeostasis.

ppk11 and *ppk16* Are Coregulated and Required for the Sustained Expression of Synaptic Homeostasis

In *GluRIIA* mutant animals, synaptic homeostasis persists over several days of larval development. We reasoned that if *ppk11* and *ppk16* are instructive for synaptic homeostasis, their transcription might be increased in *GluRIIA* mutants compared to wild-type animals. Indeed, we found that the expression of both *ppk11* and *ppk16* mRNA are increased ~4-fold in the *GluRIIA* mutant background compared to wild-type, as assessed by qPCR (Figure 6C; see Experimental Procedures). PPK11 and PPK16 are motoneuron proteins, necessary for homeostatic plasticity, that show a regulated change in gene expression that correlates with homeostatic plasticity.

We also noted that these genes show an identical increase in expression in the *GluRIIA* mutant. Since the *ppk11* and *ppk16* genes are separated by only 63 base pairs, we considered the possibility that these genes might be cotranscribed. To test this idea, we generated PCR primers that could specifically amplify either full-length *ppk11*, *ppk16*, or both genes together as part of a single transcript. We find that we are able to isolate full-length cDNAs for *ppk11*, *ppk16*, and a cDNA that spans the coding regions of both *ppk11* and *ppk16* and is of the expected size for a transcript containing both *ppk11* and *ppk16* (Figure 6D). The identity of the joint *ppk11-ppk16* transcript was confirmed by sequencing the junction between the *ppk11* and *ppk16* genes. A stop codon is present in the joint cDNA following the *ppk11* coding sequence, suggesting that the two genes are cotranscribed and translated as independent proteins. This result is reproducible across three independently derived cDNA libraries (data not shown). These data indicate that *ppk11* and *ppk16* are cotranscribed and coregulated during synaptic homeostasis, further suggesting that they could be subunits of a single channel that is upregulated during the sustained expression of synaptic homeostasis.

ppk11 and *ppk16* Represent a Single Functional Genetic Unit with Respect to Synaptic Homeostasis

We next asked whether *ppk11* and *ppk16* are not only cotranscribed and coregulated during synaptic homeostasis, but whether they function as part of a single genetic unit during synaptic homeostasis. If two genes function as part of a single genetic unit, then disrupting the expression of one gene will also affect the other gene. To test this, we performed a series of complementation experiments, diagrammed in Figure 6F. First, we show that heterozygous mutations in either the *ppk11* (+,*ppk11*^{PBac}/+,+) or the *ppk16* genes (*ppk16*^{Mi},+/+,+) do not alter synaptic homeostasis (Figures 6E and 6F). Next, we demonstrate that a heterozygous deficiency that encompasses both *ppk11* and *ppk16* (*ppk16*^{Df},*ppk11*^{Df}/+,+) also does not alter synaptic homeostasis (Figures 6E and 6F). Therefore, animals that harbor one functional copy of *ppk11* and one functional copy of *ppk16* can express normal synaptic homeostasis. However, when the heterozygous +,*ppk11*^{Pbac}/+,+ mutation is placed in *trans* to the heterozygous *ppk16*^{Mi},+/+,+ mutation

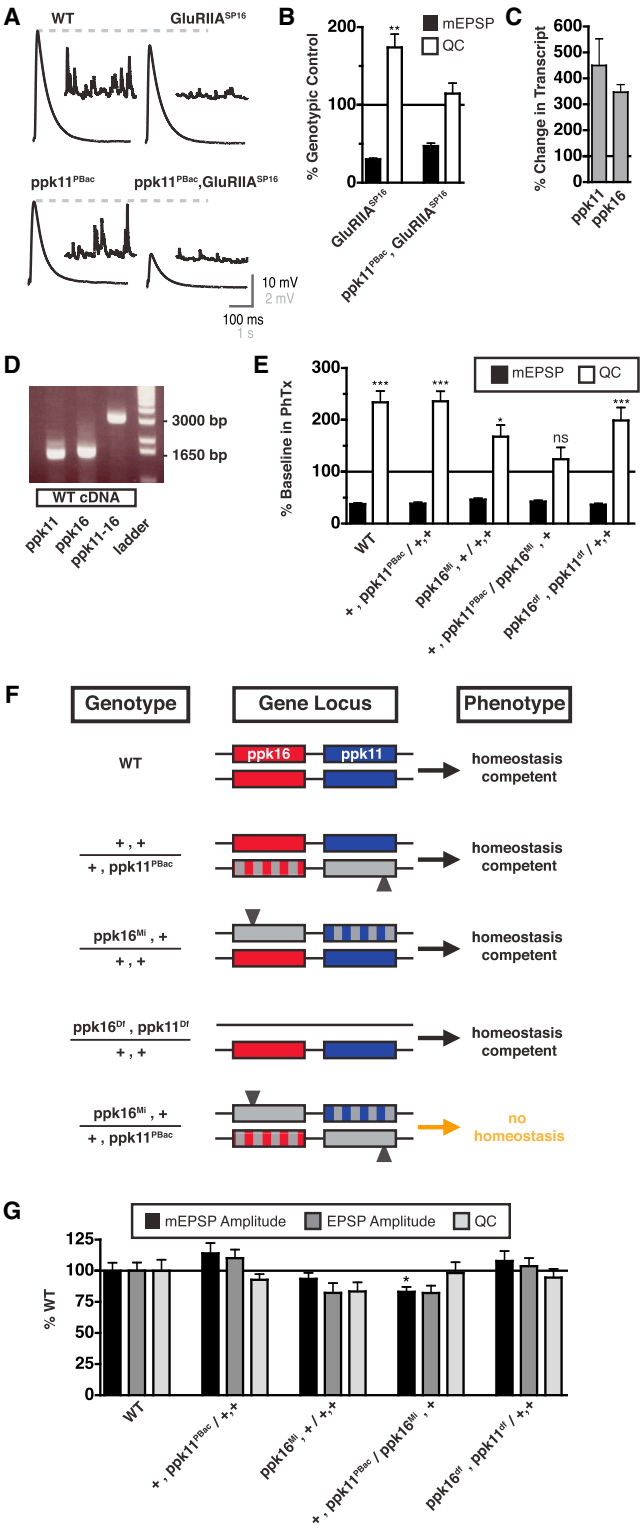

Figure 6. Pickpocket Function and Regulation during the Long-Term Expression of Synaptic Homeostasis

(A) Representative traces for indicated genotypes.

(B) mEPSP amplitude and quantal content (QC) are shown as percent baseline for each genotype. *GluRIIA*^{SP16} is shown as percent change relative to wild-type. The *ppk11*^{PBac}, *GluRIIA*^{SP16} double mutant is normalized to *ppk11*^{PBac} alone. mEPSP amplitudes are decreased ($p < 0.001$) in genotypes that include the *GluRIIA*^{SP16} mutation. *GluRIIA*^{SP16} shows an increase in QC ($p < 0.01$), while the *ppk11*^{PBac}, *GluRIIA*^{SP16} double mutant does not.

(C) *ppk11* and *ppk16* mRNA are increased ~4-fold in the *GluRIIA*^{SP16} mutant. Experiment was performed in triplicate.

(D) Ethidium bromide gel showing PCR products generated from a wild-type cDNA library. cDNAs of the expected size could be isolated with primers targeting *ppk11*, *ppk16*, or using primers that span the full length of both genes (*ppk11-16*).

(E) mEPSP amplitude (filled bars) and QC (open bars) are expressed as the percent change in the absence of PhTx as in Figure 1D. mEPSP amplitude is decreased after the addition of PhTx in all conditions ($p < 0.001$). QC is increased for WT ($p < 0.001$), +,*PPK11*/+,+ ($p < 0.001$), *PPK16*,+/+,+ ($p < 0.05$), and *PPK16*^{Df},*PPK11*^{Df}/+,+ ($p < 0.001$). There is no change in QC in +,*PPK11*^{PBac}/*PPK16*^{Mi},+ ($p = 0.29$).

(F) Schematic diagram of genetic epistasis experiment quantified below. The *ppk11* and *ppk16* locus is shown. A red rectangle and a blue rectangle represent a functional copy of the *ppk16* and *ppk11* genes, respectively. Gray represents a loss-of-function mutation in either gene, and stripes represent the unknown consequence of a transposon insertion.

(G) mEPSP amplitude, EPSP amplitude, and QC are shown as percent of WT. There are no significant differences from wild-type in any condition except a small decrease in mEPSP amplitude in +,*PPK11*^{PBac}/*PPK16*^{Mi},+ ($p < 0.05$). Data are presented as average ± SEM. Comparisons are made according to a Student's t test.

(+,*ppk11*^{PBac}/ *ppk16*^{Mi},+), then we find that synaptic homeostasis is completely blocked (Figures 6E and 6F). Although each mutation is heterozygous, they are resident on different chromosomes. As such, the heterozygous mutation in *ppk11* could disrupt the remaining functional copy of *ppk16* and vice versa (Figure 6F). Since homeostasis is blocked when heterozygous mutations are placed in *trans* but not when they are placed in *cis*, we conclude that one or both of the mutations must affect both *ppk11* and *ppk16*. These data argue that *ppk11* and *ppk16* are not only cotranscribed but function as a single, operon-like genetic unit, further supporting the possibility that these genes function together during synaptic homeostasis. This is further supported by our finding that the organization of the *ppk11/16* locus is conserved across multiple species of *Drosophila* (Figure S2), representing approximately 30 million years of evolutionary divergence, suggesting that the tandem placement of these genes is relevant to their regulation.

Although the *ppk11/16* locus is transcribed as a single RNA, we do not know whether these two could also be transcribed independently. This is important to consider when interpreting the results of transgenic RNAi. Specifically, this concerns whether *UAS-ppk11-RNAi* targets only the *ppk11* gene or whether it will also affect expression of cotranscribed *ppk16* and vice versa (Figures 3 and 4). One further observation is worth considering in the *trans*-heterozygous data set. When mutations in *ppk11* and *ppk16* are placed in *trans*, synaptic homeostasis is blocked but baseline synaptic transmission (in the absence of PhTx) is not statistically different from wild-type (Figure 6G). The only significant change observed is a minor decrease in mEPSP amplitude in *trans*-heterozygous mutants. These data confirm, again, that homeostatic synaptic plasticity can be blocked by disruption of the *ppk11/16* locus without a parallel change in baseline synaptic transmission.

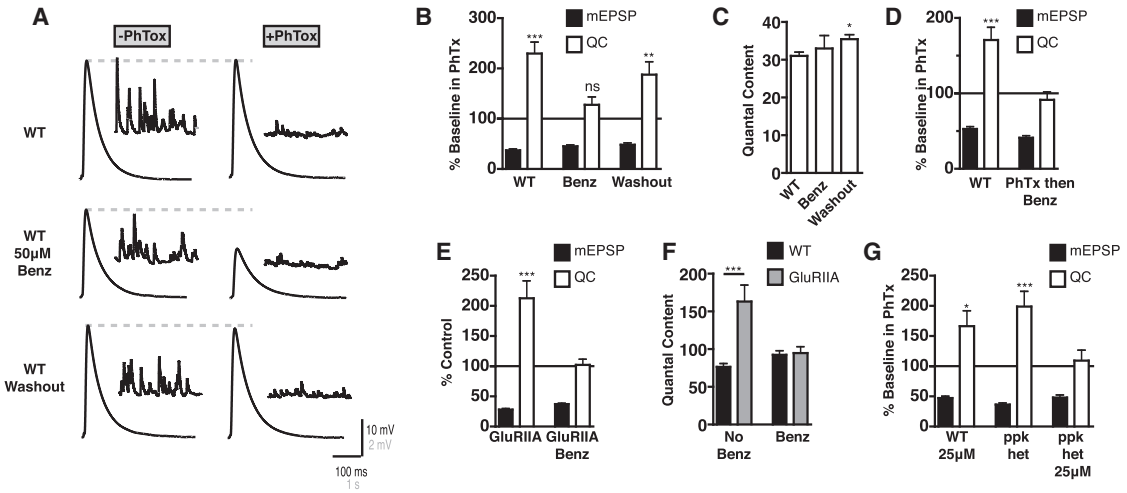

Figure 7. Pharmacological Inhibition of PPK Channels Erases the Expression of Homeostatic Plasticity

(A) Representative traces for the indicated genotypes with PhTx (right) and without PhTx (left).

(B) Percent change of mEPSP amplitude and quantal content (QC). mEPSP amplitude is decreased by PhTx in all conditions ($p < 0.001$). QC is increased in WT ($p < 0.001$) but not in the presence of 50 μM Benzamil (Benz; $p = 0.17$). QC is increased when Benzamil is washed out ($p < 0.01$).

(C) Quantal content in the absence of PhTx for each genotype in (B). Benzamil does not decrease quantal content ($p = 0.63$) and there is a slight but significant increase after Benzamil washout ($p < 0.05$).

(D) Data are represented as in (A). mEPSP amplitude is decreased by PhTx ($p < 0.001$). QC is increased in WT in the presence of PhTx ($p < 0.001$), but not when the PhTx treatment is followed by incubation in 50 μM Benzamil ($p = 0.59$).

(E) Percent change in mEPSP amplitude (filled bars) and QC (corrected for nonlinear summation; see Frank et al., 2006; open bars) in the presence of PhTx. The increase in QC observed in *GluRIIA*^{SP16} alone is prevented by 50 μM Benzamil ($p < 0.001$ without Benzamil and $p = 0.82$ with Benzamil). Recordings were made at 0.5 mM extracellular calcium.

(F) QC is shown for wild WT and *GluRIIA*^{SP16} in the absence and presence of Benzamil. There is an increase in QC in *GluRIIA*^{SP16} compared to WT ($p < 0.001$), and there is no significant difference between WT and *GluRIIA*^{SP16} in the presence of Benzamil ($p = 0.82$).

(G) Data are shown as in (B). mEPSP amplitude is decreased after the addition of PhTx in all conditions ($p < 0.001$). The PPK11-PPK16 double heterozygous (PPK het) condition in the presence of 25 μM Benzamil shows no increase in QC ($p = 0.65$). For purposes of data comparison in this panel, data for "ppk het" are identical to that presented in Figure 6E (*ppk16*^{Df}, *ppk11*^{Df}/+,+). Data are presented as average ± SEM. Comparisons are made according to a Student's t test.

PPK11/16 Channel Function Drives the Expression of Synaptic Homeostasis

We hypothesize that PPK11/16-containing DEG/ENaC channels are inserted into the presynaptic plasma membrane to cause a homeostatic increase in presynaptic release and that these channels must be maintained on the plasma membrane in order to sustain the expression of synaptic homeostasis over several days. If this is correct, then pharmacological blockade of the PPK11/16 channel conductance should erase homeostatic potentiation that was previously induced by either PhTx application or by the presence of the *GluRIIA* mutation. This appears to be the case.

DEG/ENaC channels are blocked by amiloride and its derivatives (Kleyman and Cragoe, 1988). In *Drosophila*, Benzamil has been shown to be a potent inhibitor of ENaC channel function (Liu et al., 2003a). In our first set of experiments, wild-type NMJs were coincubated in 50 μM Benzamil and 10 μM PhTx. After a 10 min incubation, recordings were made in the presence of 50 μM Benzamil. Ten minutes is normally sufficient to induce potent homeostatic compensation (Figure 7B). However, in the presence of 50 μM Benzamil, we saw a complete block in synaptic homeostasis (Figures 7A and 7B). Next, we tested whether this effect could be washed out. Benzamil reversibly blocks DEG/ENaC channels, while PhTx irreversibly antagonizes *Drosophila* glutamate receptors (Drummond et al., 1998; Frank et al., 2006). Therefore, we were able to incubate larvae in PhTx and 50 μM Benzamil for 10 min and then wash out only Benzamil, limiting its action to the time when synaptic homeostasis was induced. We saw a complete restoration of synaptic homeostasis after Benzamil was washed out. The half-maximal effective concentration for disruption of synaptic homeostasis is 32 μM (Figure S3), which is within the range expected for amiloride derivatives to act on *Drosophila* pickpocket channels (Chen et al., 2010; Boiko et al., 2012). We have also confirmed a block of synaptic homeostasis with a second amiloride derivative EIPA (5-(n-ethyl-n-isopropyl)amiloride) at 20 μM (Figure S4). From these data, we can make several conclusions. First, these data demonstrate that the conductance of the pickpocket channel is required for synaptic homeostasis, since functional blockade is sufficient to erase homeostatic plasticity. Second, since homeostasis is restored upon washout, it demonstrates that the induction process remains intact, but expression is blocked by inhibition of the DEG/ENaC channel. Third, we now have a pharmacological reagent that blocks homeostatic plasticity. Since synaptic transmission reverts to the levels seen in an uncompensated synapse when Benzamil is applied (Figure 7C), it demonstrates that synaptic homeostasis is, at least initially, a process that is layered on top of normal synaptic

transmission. Finally, in our assay, the axon is cut and only ~200 μM of axon exists between our stimulation electrode and the NMJ. Therefore, the DEG/ENaC channel must function within these 200 μM of axon or within the NMJ itself.

We next asked whether the PPK channel conductance is continuously required for the expression of synaptic homeostasis. First, Benzamil was applied after a 10 min incubation in PhTx and synaptic homeostasis was blocked (Figure 7D). Thus, ENaC channel function is necessary for the expression of synaptic homeostasis, not during the induction of the process. Next, Benzamil was applied to the *GluRIIA* mutant and, again, synaptic homeostasis was completely blocked (Figure 7E). Remarkably, quantal content in the *GluRIIA* mutant in the presence of Benzamil was identical to that observed for a wild-type NMJ in the presence of Benzamil (Figure 7F). Thus, even when synaptic homeostasis has been persistently engaged for the life of the synapse, it can be erased by blocking the function of the Benzamil-sensitive DEG/ENaC channel.

Several controls were performed. It is well established that Benzamil acts to inhibit DEG/ENaC channels (Kleyman and Cragoe, 1988; Garty and Palmer, 1997; Cuthbert and Fanelli, 1978). However, we sought additional evidence that Benzamil acts on a *Drosophila* PPK11/PPK16-containing channel. To do so, we tested whether animals that are doubly heterozygous for the *ppk11* and *ppk16* mutations (in *cis*) might have increased sensitivity to Benzamil. The double heterozygote has normal synaptic homeostasis (Figure 7G). When a low concentration of Benzamil (25 μM) is applied to a wild-type NMJ, synaptic homeostasis is also normal (Figure 7G). However, when 25 μM Benzamil is applied to the double heterozygote, synaptic homeostasis is blocked (Figure 7G). These data strongly suggest that Benzamil is acting on a DEG/ENaC channel containing PPK11 and PPK16 subunits and that inhibition of this channel is the cause of impaired synaptic homeostasis.

Finally, we note that acute application of Benzamil to the wild-type NMJ does not impair presynaptic quantal content (Figures 7B and S3). We observe a modest decrease in mEPSP amplitude but no change in quantal content. We further demonstrate that the reduction in mEPSP amplitude is an action of Benzamil that is independent of PPK11 or PPK16 and can be separated from the effect on synaptic homeostasis (Figure S3). Thus, Benzamil blocks PhTx-induced synaptic homeostasis at the wild-type NMJ without impairing baseline presynaptic release. We conclude from these data, as well as our genetic analyses, that synaptic homeostasis requires a Benzamil-sensitive DEG/ENaC channel, which is likely to include both the PPK11 and PPK16 subunits, and this channel has little or no role during baseline synaptic release in the absence of a homeostatic perturbation.

Pickpocket Channel Blockade Prevents the Homeostatic Modulation of Presynaptic Calcium Influx

It was previously demonstrated that the homeostatic modulation of presynaptic release is achieved, in part, through an increase in presynaptic calcium influx via the CaV2.1 calcium channel ortholog *cacophony* (Müller and Davis, 2012). Since Benzamil does not alter baseline presynaptic release, it is unlikely to alter calcium channel function directly. However, DEG/ENaC channels are nonvoltage-activated cation channels that show a strong preference for sodium. As such, increased DEG/ENaC channel function could depolarize the presynaptic membrane and indirectly enhance calcium channel activity, thereby increasing neurotransmitter release. This possibility is consistent with evidence that subthreshold presynaptic depolarization enhances neurotransmitter release at the NMJ (Wojtowicz and Atwood, 1983, 1984) and enhances both presynaptic calcium influx and release at central synapses (Awatramani et al., 2005).

To determine whether the PPK11/16-containing DEG/ENaC channel might influence presynaptic calcium influx through the CaV2.1 calcium channel, we imaged presynaptic spatially averaged calcium signal after single action potential stimulation with the calcium indicator Oregon Green Bapta-1 (OGB-1), as previously described (Müller and Davis 2012). First, we find that calcium influx is increased in *GluRIIA* mutant animals compared to wild-type, confirming our previously published results (Figures 8A and 8B; $p < 0.05$; see also Müller and Davis, 2012). Next, we demonstrate that application of Benzamil to the wild-type NMJ has no effect on the amplitude of the evoked calcium transient (Figures 8A and 8B). This is consistent with our conclusion based on electrophysiology that Benzamil does not alter steady-state neurotransmitter release. Finally, we show that Benzamil application to the *GluRIIA* mutant causes a pronounced decrease in the amplitude of the evoked calcium transient that could entirely account for the observed Benzamil-dependent block of synaptic homeostasis (Figure 8B; $p < 0.001$).

It should be noted that, in both wild-type and *GluRIIA* mutant animals, Benzamil causes a drop in baseline OGB-1 fluorescence (F_{base}) that is significant in wild-type and approaches significance in *GluRIIA* (Figure 8C; $p < 0.01$ and $p = 0.55$, respectively). It is likely that photobleaching during sequential acquisition of calcium transients prior to and after Benzamil application contributes to the drop in F_{base}. It remains formally possible that Benzamil influences the F_{base} measurement and we cannot rule out the possibility that baseline calcium is decreased. However, since a drop in F_{base} should, if anything, increase calcium transient amplitudes (measured as $\Delta F/F_{base}$, see Experimental Procedures), this effect cannot account for the large decrease in the amplitude of the evoked calcium transients when Benzamil is applied to the *GluRIIA* mutant. These data support the conclusion that Benzamil-dependent inhibition of the PPK11/16 containing DEG/ENaC channel blocks synaptic homeostasis by indirectly preventing the modulation of calcium influx through presynaptic CaV2.1 calcium channels. These data are consistent with a new model for homeostatic synaptic plasticity in which the induction of synaptic homeostasis drives an increase in pickpocket channel function at or near the presynaptic membrane, possibly through the insertion of new channels (Figure 8D; see Discussion).

DISCUSSION

We provide evidence that a presynaptic DEG/ENaC channel composed of PPK11 and PPK16 is required for the rapid induction, expression, and continued maintenance of homeostatic synaptic plasticity at the *Drosophila* NMJ. Remarkably, *ppk11* and *ppk16* genes are not only required for homeostatic plasticity

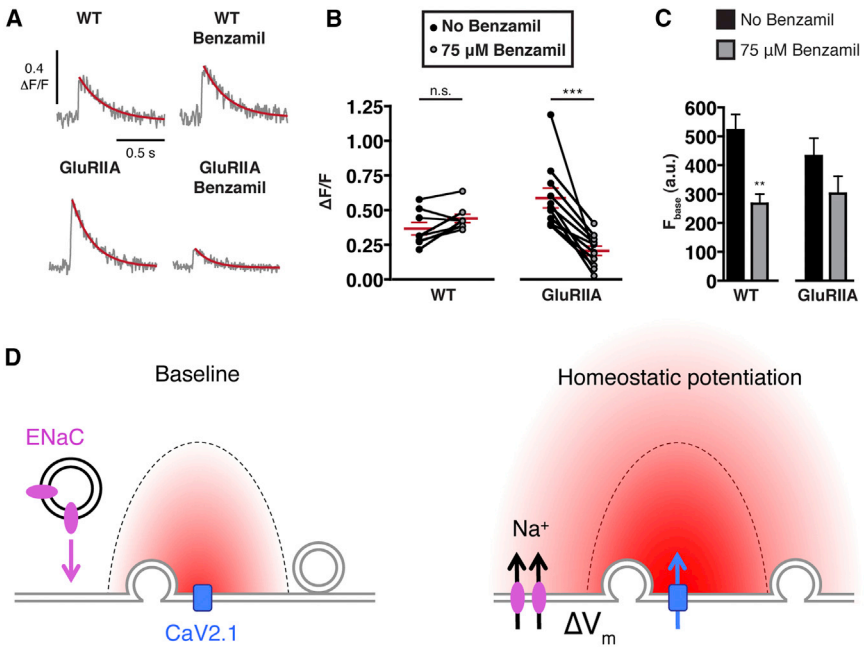

Figure 8. A Model for PPK11/16 Function during Synaptic Homeostasis

(A) Representative traces of single action potential-evoked spatially averaged calcium transients (average of eight to ten scans each) for the indicated genotypes with and without Benzamil (right and left, respectively).

(B) ΔF/F calcium transient peak amplitudes for individual boutons imaged before and after 75 μM Benzamil application (n = 8 and n = 11 boutons for wild-type [WT] and the *GluRIIA* mutant, respectively). There is no significant change in ΔF/F in WT after Benzamil treatment ($p = 0.07$), and there is a significant decrease in the *GluRIIA* mutant after Benzamil treatment ($p < 0.001$).

(C) Average baseline fluorescence (F_{base}) for WT and GluRIIA in the presence and absence of Benzamil. There is a statistically significant decrease in WT after Benzamil treatment ($p < 0.01$) and a nonsignificant trend toward a decrease in *GluRIIA* treated with Benzamil ($p = 0.055$).

(D) Our data support a model whereby PPK11- and PPK16-containing channels (purple) are inserted into the presynaptic membrane during synaptic homeostasis to cause an increase in sodium influx and a resulting change in presynaptic resting potential ΔVm (right). The change in presynaptic resting potential directly or indirectly leads to increased presynaptic calcium influx (red). Data are presented as average ± SEM. Comparisons are made according to a Student's t test.

but are among the first homeostatic plasticity genes shown to be differentially regulated during homeostatic plasticity. Specifically, we show that expression of both *ppk11* and *ppk16* is increased 4-fold in the *GluRIIA* mutant background. We also demonstrate that *ppk11* and *ppk16* are transcribed together in a single transcript and behave genetically as an operon-like, single genetic unit. This molecular organization suggests a model in which *ppk11* and *ppk16* are cotranscribed to generate DEG/ENaC channels with an equal stoichiometric ratio of PPK11 and PPK16 subunits. This is consistent with previous models for gene regulation in *Drosophila* (Blumenthal, 2004). However, we cannot rule out the possibility that two independent DEG/ENaC channels are upregulated, one containing PPK11 and one containing PPK16. The upregulation of *ppk11* and *ppk16* together with the necessity of DEG/ENaC channel function during the time when synaptic homeostasis is assayed, indicates that these genes are probably part of the homeostat and not merely necessary for the expression of synaptic homeostasis.

A Model for DEG/ENaC Channel Function during Homeostatic Plasticity

DEG/ENaC channels are voltage-insensitive cation channels that are primarily permeable to sodium (Ben-Shahar, 2011; Bianchi and Driscoll, 2002) and can carry a sodium leak current. A model for DEG/ENaC channel function during synaptic homeostasis can be based on the well-established regulation of ENaC channel trafficking in the kidney during the homeostatic control of salt balance. Enhanced sodium reabsorption in the principle cells of the cortical collecting duct of the kidney is triggered by aldosterone binding to the mineralocorticoid receptor. This increases ENaC channel transcription and trafficking to the apical cell surface, which enhances sodium influx. Sodium is then pumped out of the basolateral side of the cell, accomplishing sodium reabsorption (Schild, 2010).

We speculate that a retrograde, homeostatic signal from muscle triggers increased trafficking of a PPK11/16-containing DEG/ENaC channel to the neuronal plasma membrane, at or near the NMJ. Since the rapid induction of synaptic homeostasis is protein synthesis independent (Goold and Davis, 2007), we hypothesize the existence of a resting pool of PPK11/16 channels that are inserted in the membrane in response to postsynaptic glutamate receptor inhibition. If postsynaptic glutamate receptor inhibition is sustained, as in the *GluRIIA* mutant, then increased transcription of *ppk11/16* supports a persistent requirement for this channel at the developing NMJ. Once on the plasma membrane, the PPK11/16 channel would induce a sodium leak and cause a moderate depolarization of the nerve terminal. This subthreshold depolarization would lead, indirectly, to an increase in action potential-induced presynaptic calcium influx through the CaV2.1 calcium channel and subsequent neurotransmitter release (Figure 8D).

There are two major possibilities for how ENaC-dependent depolarization of the nerve terminal could potentiate calcium influx and evoked neurotransmitter release. One possibility, based on work in the ferret prefrontal cortex and *Aplysia* central synapses (Shu et al., 2006; Shapiro et al., 1980), is that presynaptic membrane depolarization causes action potential broadening through potassium channel inactivation, thereby enhancing both calcium influx and release. A second possibility is that subthreshold depolarization of the nerve terminal causes an increase in resting calcium that leads to calcium-dependent calcium channel facilitation (Cuttle et al., 1998; Borst and

Sakmann, 1998). Consistent with this model, it has been shown at several mammalian synapses that subthreshold depolarization of the presynaptic nerve terminal increases resting calcium and neurotransmitter release through low-voltage modulation of presynaptic P/Q-type calcium channels (Awatramani et al., 2005; Alle and Geiger, 2006; Christie et al., 2011). However, at these mammalian synapses, the change in resting calcium does not lead to an increase in action potential-evoked calcium influx, highlighting a difference between the mechanisms of homeostatic potentiation and the type of presynaptic modulation observed at these other synapses (Awatramani et al., 2005; Alle and Geiger, 2006; Christie et al., 2011). The mechanism by which elevated basal calcium potentiates release at these mammalian synapses remains under debate (Bouhours et al., 2011; Chu et al., 2012). It should be noted that small, subthreshold depolarization of the presynaptic resting potential, as small as 5 mV, are sufficient to cause a 2-fold increase in release at both neuromuscular (Wojtowicz and Atwood, 1983) and mammalian central synapses (Awatramani et al., 2005; Christie et al., 2011). This is within a reasonable range for modulation of presynaptic membrane potential by pickpocket channel insertion. Unfortunately, it is not technically feasible to record directly from the presynaptic terminal at the *Drosophila* NMJ. Finally, we note that it remains formally possible that a PPK11/16-containing DEG/ENaC channel passes calcium, based upon the ability of mammalian ASIC channels to flux calcium (Waldmann et al., 1997).

This model might provide insight regarding how accurate tuning of presynaptic neurotransmitter release can be achieved (Frank et al., 2006). There is a supralinear relationship between calcium influx and release (Katz and Miledi, 1970; Bollmann et al., 2000; Schneggenburger and Neher, 2000). Therefore, if changing calcium channel number is the mechanism by which synaptic homeostasis is achieved, then there must be very tight and tunable control of calcium channel number within each presynaptic active zone. By contrast, if homeostatic plasticity is achieved by ENaC-dependent modulation of membrane voltage, then variable insertion of ENaC channels could uniformly modulate calcium channel activity, simultaneously across all of the active zones of the presynaptic nerve terminal. Furthermore, if the ENaC channel sodium leak is small, and if presynaptic calcium channels are moderately influenced by small changes in resting membrane potential, then relatively coarse modulation of ENaC channel trafficking could be used to achieve precise, homeostatic control of calcium influx and neurotransmitter release. Again, these are testable hypotheses that will be addressed in the future.

EXPERIMENTAL PROCEDURES

Electrophysiology

Recordings were made from muscle 6 in abdominal segments 2 and 3 from third-instar larvae, as previously described (Frank et al., 2006, 2009, Müller et al., 2012). Recordings were made in HL3 saline containing 70 mM NaCl, 5 mM KCl, 10 mM $MgCl_2$, 10 mM $NaHCO_3$, 115 mM sucrose, 4.2 mM trehalose, 5 mM HEPES, and 0.35 mM $CaCl_2$, unless otherwise specified. Quantal content was calculated by dividing the average EPSP amplitude by the average mEPSP amplitude for each muscle recording. Where specified, quantal content was corrected for nonlinear summation (NLS) according to established methods (Martin, 1955; Davis and Goodman, 1998). For acute pharmacological homeostatic challenge, larvae were incubated in Philanthotoxin-433 (PhTx; 10–20 μM; Sigma-Aldrich) for 10 min (Frank et al., 2006). Benzamil hydrochoride hydrate (Sigma-Aldrich) was prepared as a stock in H_2O and diluted to the desired concentration in HL3 saline. EIPA (5-(n-ethyl-n-isopropyl)amiloride; Sigma-Aldrich) was prepared as a stock in DMSO, then diluted 1:1,000 in HL3 to a concentration of EIPA of 20 μM. A 1:1,000 dilution of DMSO is without effect on synaptic transmission (Frank et al., 2006).

Two-electrode voltage-clamp recordings were done as previously described (Müller et al., 2012). All recordings were made from muscle 6 in abdominal segments 2 and 3 from third-instar larvae in HL3 saline with 1 mM $CaCl_2$. mEPSPs were recorded with the amplifier in bridge mode before switching to TEVC mode. mEPSPs were analyzed rather than mEPSCs, because of the low signal-to-noise ratio for mEPSCs. EPSC analysis was conducted using custom-written routines for Igor Pro 5.0 (WaveMetrics), and mEPSPs were analyzed using Mini Analysis 6.0.0.7 (Synaptosoft).

Fly Stocks and Genetics

In all experiments, the w^{1118} strain was used at the wild-type control, and animals were raised at 22°C, unless otherwise noted. *Drosophila melanogaster* stocks with the following mutations, *UAS*-transgenes, or *GAL4* drivers were used in the course of this study: *UAS-ppk11-RNAi*, *UAS-ppk11-dn*, and *UAS-ppk19-RNAi* were the kind gifts of Lei Liu. $ppk11^{MI}$, $ppk11^{PBac}$, $ppk16^{MI}$, and *Df(2l)BSC240* (PPK deficiency) were acquired from the Bloomington Stock Center. *UAS-ppk16-RNAi* was acquired from the Vienna Drosophila Stock Center (VDRC transformant ID 22990). The $GluRIIA^{SP16}$ null mutation (Petersen et al., 1997), the *OK371-GAL4* driver (Mahr and Aberle, 2006), and the *MHC-Gal4* driver (Schuster et al., 1996) have all been previously reported on. The precise excision, $ppk11^{Precise}$, and the imprecise excision, $ppk16^{166}$, were generated according to standard procedures (Metaxakis et al., 2005). Deletions were identified by PCR, and all results were verified through sequencing.

Anatomical Analysis

Third-instar larval preparations were fixed in Bouin's fixative, washed, and incubated overnight at 4°C in primary antibodies. Secondary antibodies were applied at room temperature for 2 hr. The following antibodies were used: anti-NC82 (1:100; mouse; Developmental Studies Hybridoma Bank) and anti-DLG (1:10,000; rabbit). Alexa-conjugated secondary antibodies and Cy5-conjugated goat ant-HRP were used at 1:250 (Jackson ImmunoResearch Laboratories; Molecular Probes). Larval preparations were mounted in Vectashield (Vector) and imaged at room temperature using an Axiovert 200 (Zeiss) inverted microscope, a 100× Plan Apochromat objective (1.4 NA), and a cooled charge-coupled device camera (Coolsnap HQ, Roper). Intelligent Imaging Innovations (3I) software was used to capture, process, and analyze images.

CNS Quantitative RT-PCR

RT-PCR was performed as previously described (Bergquist et al., 2010). Primer-probes specific for real-time PCR detection of *ppk11*, *ppk16*, and Ribosomal protein L32 (*RpL32*) were designed and developed by Applied Biosystems. The CNS was removed from 25 third-instar larvae per sample (three samples/genotype). Total RNA was isolated from each sample using the standard Trizol protocol. A DNase digestion removed potential DNA contamination (RQ1 RNase-free DNase Promega).

cDNA Extraction and Amplification

cDNA libraries were generated using the SMARTer RACE cDNA Amplification Kit (Clontech). Primers used for PPK11 and PPK16 amplification were as follows: ppk11 forward, 5′-ATGTCCGACGTTCCAGGAG-3′; ppk11 reverse, 5′-ATTAGCCGGCCCTAATGACC-3′; ppk16 forward, 5′-ATGGCTTTCAA GAAGCGGCG-3′; ppk16 reverse, 5′-CTACTCCCGGTTGATGTAGTT-3′. PCR was done using TAQ polymerase, according to standard procedures.

Calcium Imaging

Ca^{2+} imaging experiments were done as described in Müller and Davis (2012). See Supplemental Experimental Procedures for details regarding dissection, dye loading, and imaging.

SUPPLEMENTAL INFORMATION

Supplemental Information includes Supplemental Experimental Procedures, four figures, and two tables and can be found with this article online at http://dx.doi.org/10.1016/j.neuron.2013.06.048.

ACKNOWLEDGMENTS

This study was supported by NIH grant number NS39313 to G.W.D. We thank Li Liu for sending *Drosophila* stocks and Susan Younger, Phil Parker, Kevin Ford, and members of the Davis laboratory for help and advice.

Accepted: June 24, 2013
Published: August 22, 2013

REFERENCES

Adams, C.M., Anderson, M.G., Motto, D.G., Price, M.P., Johnson, W.A., and Welsh, M.J. (1998). Ripped pocket and pickpocket, novel Drosophila DEG/ENaC subunits expressed in early development and in mechanosensory neurons. J. Cell Biol. *140*, 143–152.

Alle, H., and Geiger, J.R.P. (2006). Combined analog and action potential coding in hippocampal mossy fibers. Science *311*, 1290–1293.

Awatramani, G.B., Price, G.D., and Trussell, L.O. (2005). Modulation of transmitter release by presynaptic resting potential and background calcium levels. Neuron *48*, 109–121.

Ben-Shahar, Y. (2011). Sensory functions for degenerin/epithelial sodium channels (DEG/ENaC). Adv. Genet. *76*, 1–26.

Benson, C.J., Xie, J., Wemmie, J.A., Price, M.P., Henss, J.M., Welsh, M.J., and Snyder, P.M. (2002). Heteromultimers of DEG/ENaC subunits form H+-gated channels in mouse sensory neurons. Proc. Natl. Acad. Sci. USA *99*, 2338–2343.

Bergquist, S., Dickman, D.K., and Davis, G.W. (2010). A hierarchy of cell intrinsic and target-derived homeostatic signaling. Neuron *66*, 220–234.

Bernard, C., Anderson, A., Becker, A., Poolos, N.P., Beck, H., and Johnston, D. (2004). Acquired dendritic channelopathy in temporal lobe epilepsy. Science *305*, 532–535.

Bianchi, L., and Driscoll, M. (2002). Protons at the gate: DEG/ENaC ion channels help us feel and remember. Neuron *34*, 337–340.

Blumenthal, T. (2004). Operons in eukaryotes. Brief. Funct. Genomics Proteomics *3*, 199–211.

Boiko, N., Kucher, V., Stockand, J.D., and Eaton, B.A. (2012). Pickpocket1 is an ionotropic molecular sensory transducer. J. Biol. Chem. *287*, 39878–39886.

Bollmann, J.H., Sakmann, B., and Borst, J.G. (2000). Calcium sensitivity of glutamate release in a calyx-type terminal. Science *289*, 953–957.

Borst, J.G., and Sakmann, B. (1998). Facilitation of presynaptic calcium currents in the rat brainstem. J. Physiol. *513*, 149–155.

Bouhours, B., Trigo, F.F., and Marty, A. (2011). Somatic depolarization enhances GABA release in cerebellar interneurons via a calcium/protein kinase C pathway. J. Neurosci. *31*, 5804–5815.

Chalfie, M. (2009). Neurosensory mechanotransduction. Nat. Rev. Mol. Cell Biol. *10*, 44–52.

Chandrashekar, J., Kuhn, C., Oka, Y., Yarmolinsky, D.A., Hummler, E., Ryba, N.J., and Zuker, C.S. (2010). The cells and peripheral representation of sodium taste in mice. Nature *464*, 297–301.

Chen, Z., Wang, Q., and Wang, Z. (2010). The amiloride-sensitive epithelial Na+ channel PPK28 is essential for drosophila gustatory water reception. J. Neurosci. *30*, 6247–6252.

Christie, J.M., Chiu, D.N., and Jahr, C.E. (2011). Ca(2+)-dependent enhancement of release by subthreshold somatic depolarization. Nat. Neurosci. *14*, 62–68.

Chu, Y., Fioravante, D., Thanawala, M., Leitges, M., and Regehr, W.G. (2012). Calcium-dependent isoforms of protein kinase C mediate glycine-induced synaptic enhancement at the calyx of Held. J. Neurosci. *32*, 13796–13804.

Cuthbert, A.W., and Fanelli, G.M. (1978). Effects of some pyrazinecarboxamides on sodium transport in frog skin. Br. J. Pharmacol. *63*, 139–149.

Cuttle, M.F., Tsujimoto, T., Forsythe, I.D., and Takahashi, T. (1998). Facilitation of the presynaptic calcium current at an auditory synapse in rat brainstem. J. Physiol. *512*, 723–729.

Davis, G.W. (2006). Homeostatic control of neural activity: from phenomenology to molecular design. Annu. Rev. Neurosci. *29*, 307–323.

Davis, G.W., and Bezprozvanny, I. (2001). Maintaining the stability of neural function: a homeostatic hypothesis. Annu. Rev. Physiol. *63*, 847–869.

Davis, G.W., and Goodman, C.S. (1998). Synapse-specific control of synaptic efficacy at the terminals of a single neuron. Nature *392*, 82–86.

Davis, G.W., Schuster, C.M., and Goodman, C.S. (1997). Genetic analysis of the mechanisms controlling target selection: target-derived Fasciclin II regulates the pattern of synapse formation. Neuron *19*, 561–573.

DiAntonio, A., Petersen, S.A., Heckmann, M., and Goodman, C.S. (1999). Glutamate receptor expression regulates quantal size and quantal content at the Drosophila neuromuscular junction. J. Neurosci. *19*, 3023–3032.

Dickman, D.K., and Davis, G.W. (2009). The schizophrenia susceptibility gene dysbindin controls synaptic homeostasis. Science *326*, 1127–1130.

Drummond, H.A., Price, M.P., Welsh, M.J., and Abboud, F.M. (1998). A molecular component of the arterial baroreceptor mechanotransducer. Neuron *21*, 1435–1441.

Frank, C.A., Kennedy, M.J., Goold, C.P., Marek, K.W., and Davis, G.W. (2006). Mechanisms underlying the rapid induction and sustained expression of synaptic homeostasis. Neuron *52*, 663–677.

Frank, C.A., Pielage, J., and Davis, G.W. (2009). A presynaptic homeostatic signaling system composed of the Eph receptor, ephexin, Cdc42, and CaV2.1 calcium channels. Neuron *61*, 556–569.

Garty, H., and Palmer, L.G. (1997). Epithelial sodium channels: function, structure, and regulation. Physiol. Rev. *77*, 359–396.

Gonzalez-Islas, C., Chub, N., Garcia-Bereguiain, M.A., and Wenner, P. (2010). GABAergic synaptic scaling in embryonic motoneurons is mediated by a shift in the chloride reversal potential. J. Neurosci. *30*, 13016–13020.

Goold, C.P., and Davis, G.W. (2007). The BMP ligand Gbb gates the expression of synaptic homeostasis independent of synaptic growth control. Neuron *56*, 109–123.

Houweling, A.R., Bazhenov, M., Timofeev, I., Steriade, M., and Sejnowski, T.J. (2005). Homeostatic synaptic plasticity can explain post-traumatic epileptogenesis in chronically isolated neocortex. Cereb. Cortex *15*, 834–845.

Jakubs, K., Nanobashvili, A., Bonde, S., Ekdahl, C.T., Kokaia, Z., Kokaia, M., and Lindvall, O. (2006). Environment matters: synaptic properties of neurons born in the epileptic adult brain develop to reduce excitability. Neuron *52*, 1047–1059.

Jasti, J., Furukawa, H., Gonzales, E.B., and Gouaux, E. (2007). Structure of acid-sensing ion channel 1 at 1.9 A resolution and low pH. Nature *449*, 316–323.

Kamenetz, F., Tomita, T., Hsieh, H., Seabrook, G., Borchelt, D., Iwatsubo, T., Sisodia, S., and Malinow, R. (2003). APP processing and synaptic function. Neuron *37*, 925–937.

Katz, B., and Miledi, R. (1970). Further study of the role of calcium in synaptic transmission. J. Physiol. *207*, 789–801.

Kim, S.H., and Ryan, T.A. (2010). CDK5 serves as a major control point in neurotransmitter release. Neuron *67*, 797–809.

Kleyman, T.R., and Cragoe, E.J., Jr. (1988). Amiloride and its analogs as tools in the study of ion transport. J. Membr. Biol. *105*, 1–21.

Liu, L., Johnson, W.A., and Welsh, M.J. (2003a). Drosophila DEG/ENaC pickpocket genes are expressed in the tracheal system, where they may be involved in liquid clearance. Proc. Natl. Acad. Sci. USA *100*, 2128–2133.

Liu, L., Leonard, A.S., Motto, D.G., Feller, M.A., Price, M.P., Johnson, W.A., and Welsh, M.J. (2003b). Contribution of Drosophila DEG/ENaC genes to salt taste. Neuron *39*, 133–146.

Mahr, A., and Aberle, H. (2006). The expression pattern of the Drosophila vesicular glutamate transporter: a marker protein for motoneurons and glutamatergic centers in the brain. Gene Expr. Patterns *6*, 299–309.

Marder, E., and Goaillard, J.-M. (2006). Variability, compensation and homeostasis in neuron and network function. Nat. Rev. Neurosci. *7*, 563–574.

Martin, A.R. (1955). A further study of the statistical composition on the end-plate potential. J. Physiol. *130*, 114–122.

Metaxakis, A., Oehler, S., Klinakis, A., and Savakis, C. (2005). Minos as a genetic and genomic tool in Drosophila melanogaster. Genetics *171*, 571–581.

Müller, M., and Davis, G.W. (2012). Transsynaptic control of presynaptic Ca^{2+} influx achieves homeostatic potentiation of neurotransmitter release. Curr. Biol. *22*, 1102–1108.

Müller, M., Pym, E.C., Tong, A., and Davis, G.W. (2011). Rab3-GAP controls the progression of synaptic homeostasis at a late stage of vesicle release. Neuron *69*, 749–762.

Müller, M., Liu, K.S., Sigrist, S.J., and Davis, G.W. (2012). RIM controls homeostatic plasticity through modulation of the readily-releasable vesicle pool. J. Neurosci. *32*, 16574–16585.

Petersen, S.A., Fetter, R.D., Noordermeer, J.N., Goodman, C.S., and DiAntonio, A. (1997). Genetic analysis of glutamate receptors in Drosophila reveals a retrograde signal regulating presynaptic transmitter release. Neuron *19*, 1237–1248.

Piedras-Rentería, E.S., Pyle, J.L., Diehn, M., Glickfeld, L.L., Harata, N.C., Cao, Y., Kavalali, E.T., Brown, P.O., and Tsien, R.W. (2004). Presynaptic homeostasis at CNS nerve terminals compensates for lack of a key Ca2+ entry pathway. Proc. Natl. Acad. Sci. USA *101*, 3609–3614.

Plomp, J.J., van Kempen, G.T., and Molenaar, P.C. (1992). Adaptation of quantal content to decreased postsynaptic sensitivity at single endplates in alpha-bungarotoxin-treated rats. J. Physiol. *458*, 487–499.

Ramocki, M.B., and Zoghbi, H.Y. (2008). Failure of neuronal homeostasis results in common neuropsychiatric phenotypes. Nature *455*, 912–918.

Schild, L. (2010). The epithelial sodium channel and the control of sodium balance. Biochim. Biophys. Acta *1802*, 1159–1165.

Schneggenburger, R., and Neher, E. (2000). Intracellular calcium dependence of transmitter release rates at a fast central synapse. Nature *406*, 889–893.

Schuster, C.M., Davis, G.W., Fetter, R.D., and Goodman, C.S. (1996). Genetic dissection of structural and functional components of synaptic plasticity. II. Fasciclin II controls presynaptic structural plasticity. Neuron *17*, 655–667.

Shapiro, E., Castellucci, V.F., and Kandel, E.R. (1980). Presynaptic membrane potential affects transmitter release in an identified neuron in Aplysia by modulating the Ca2+ and K+ currents. Proc. Natl. Acad. Sci. USA *77*, 629–633.

Shu, Y., Hasenstaub, A., Duque, A., Yu, Y., and McCormick, D.A. (2006). Modulation of intracortical synaptic potentials by presynaptic somatic membrane potential. Nature *441*, 761–765.

Thiagarajan, T.C., Lindskog, M., Malgaroli, A., and Tsien, R.W. (2007). LTP and adaptation to inactivity: overlapping mechanisms and implications for metaplasticity. Neuropharmacology *52*, 156–175.

Turrigiano, G.G. (2008). The self-tuning neuron: synaptic scaling of excitatory synapses. Cell *135*, 422–435.

Wagh, D.A., Rasse, T.M., Asan, E., Hofbauer, A., Schwenkert, I., Dürrbeck, H., Buchner, S., Dabauvalle, M.C., Schmidt, M., Qin, G., et al. (2006). Bruchpilot, a protein with homology to ELKS/CAST, is required for structural integrity and function of synaptic active zones in Drosophila. Neuron *49*, 833–844.

Waldmann, R., Champigny, G., Bassilana, F., Heurteaux, C., and Lazdunski, M. (1997). A proton-gated cation channel involved in acid-sensing. Nature *386*, 173–177.

Weyhersmüller, A., Hallermann, S., Wagner, N., and Eilers, J. (2011). Rapid active zone remodeling during synaptic plasticity. J. Neurosci. *31*, 6041–6052.

Wojtowicz, J.M., and Atwood, H.L. (1983). Maintained depolarization of synaptic terminals facilitates nerve-evoked transmitter release at a crayfish neuromuscular junction. J. Neurobiol. *14*, 385–390.

Wojtowicz, J.M., and Atwood, H.L. (1984). Presynaptic membrane potential and transmitter release at the crayfish neuromuscular junction. J. Neurophysiol. *52*, 99–113.

Zhao, C., Dreosti, E., and Lagnado, L. (2011). Homeostatic synaptic plasticity through changes in presynaptic calcium influx. J. Neurosci. *31*, 7492–7496.